ARTIFICIAL NEURAL NETWORK-BASED PERFORMANCE ENHANCEMENT OF GRID-CONNECTED PV SYSTEM

Chandra Prakash Jain[1]*, Prof (Dr.) Vinesh Agarwal[2], Prakash Sundaram[3], Dr. Ritesh Tirole[4]

Abstract:
Solar energy has emerged as a significant renewable energy source due to its abundant and freely available nature. Among the different renewable energy sources, solar energy holds great importance. In solar-based systems, an MPPT (Maximum Power Point Tracking) controller plays a crucial role in extracting the maximum power available under specific irradiance and temperature conditions. The utilization of artificial intelligence (AI) is steadily increasing across various sectors of photovoltaic (PV) systems. This growth can be attributed to advancements in computing power, tools, and data generation. Several functions within the solar PV industry, including design, forecasting, control, and maintenance, currently rely on methods that often yield inaccurate results. By delving into these aspects, this study aims to shed light on the role of AI in enhancing the efficiency and effectiveness of various stages within the PV value chain. Through careful analysis, it seeks to provide valuable insights into the potential benefits and drawbacks associated with the integration of AI in solar PV systems.

[1*]Research Scholar, Department of Electrical Engineering, Sangam University, Rajasthan, India
[2]Professor, Department of Electrical Engineering, Sangam University, Rajasthan, India
[3]Associate Professor, Department of Electrical Engineering, Vidya Bhawan Polytechnic College, Rajasthan, India
[4]Assistant Professor, Department of Electrical Engineering, Sir Padampat Singhania University, Rajasthan, India

DOI: 10.31838/ecb/2022.11.11.37

INTRODUCTION

In recent times, the demand for energy has been rapidly increasing due to factors such as population growth, urbanization, and industrialization. One of the prominent challenges faced today is maintaining power system stability. Power system stability refers to the ability of a power system to maintain operational equilibrium after being subjected to disturbances under given initial conditions [1]. It is crucial to uphold power system stability in order to ensure the secure and uninterrupted operation of the system. Instances of major blackouts resulting from power system instability have prompted scientists and researchers to explore methods for improving system stability (Wollenberg et al., 2004; Wei et al., 2006; Sulzberger et al., 2006).

In recent years, the power system has experienced an increasing burden and stress compared to the past. Several factors have contributed to this situation, including the growing interconnections between power systems [2], the rapid adoption of new technologies to enhance power transmission on existing infrastructure, long-distance bulk power transmission, a significant penetration of renewable energy sources, and the widespread use of induction machines. Building new power transmission lines to meet the rising demand is not economically viable, which has led to the overloading of existing lines. This, in turn, results in voltage instability. Voltage instability occurs when the voltage exceeds or falls below a nominal value for a certain period. Over-voltage, or voltage swell, leads to excessive voltage, while under-voltage, or voltage sag, causes reduced voltage conditions. To address these issues, various devices classified under the umbrella term FACTS (Flexible AC transmission system) are employed. These FACTS devices include DSTATCOM, SVCs, SSSC, and UPFC, among others.

Ensuring fault analysis in solar photovoltaic (PV) arrays is essential for enhancing reliability, efficiency, and safety in PV systems. Undetected faults in PV arrays can not only diminish power generation and accelerate system aging but also jeopardize the overall availability of the system [3]. Detecting faults in PV arrays can be challenging due to the current-limiting nature and nonlinear output characteristics of the arrays. Moreover, faults in other components of the power system, such as Maximum Power Point Tracking (MPPT), Voltage Source Inverters, and the grid, can also impact the output power of the PV system, leading to performance degradation.

ARTIFICIAL NEURAL NETWORK

Electrical power systems are prone to unexpected faults caused by various random factors. These faults pose a significant threat to the continuity and security of electricity supply. To safeguard the system, it is crucial to detect and isolate faults promptly. This is accomplished through the use of devices capable of sensing faults and quickly reacting to disconnect the faulty section. Numerous techniques exist for online fault detection, including conventional methods and artificial methods. Conventional methods often exhibit slower response times due to the involvement of mechanical components. To overcome this limitation, Artificial Neural Networks (ANNs) are employed, as they offer the advantage of training with offline data and subsequent use for online fault detection (Tayeb et al., 2013).

Artificial Intelligence (AI) involves the simulation of human intelligence in machines, encompassing processes such as reasoning, learning, and self-correction. An Artificial Neural Network (ANN) is a computational system that emulates the structure and function of a biological neural network. Various types of neural networks exist, depending on the structure of the brain's neurons and network function. In below Figure illustrates the different possible types of neural networks [4]. Two main categories of neural networks are based on the connections between input, output, and hidden layers: feed-forward networks and feed-back networks (recurrent networks).

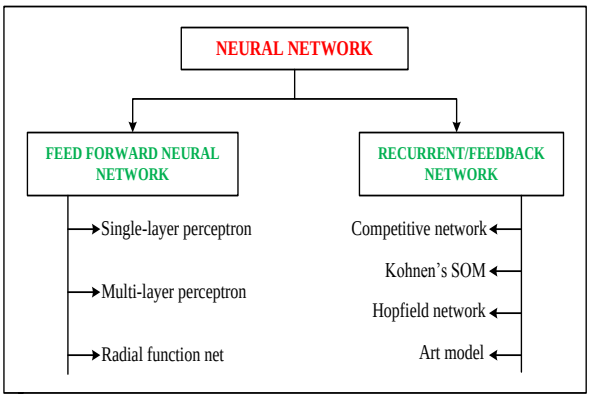

Fig 01: Classification of Neural Network

Feed-forward neural network: A feed-forward neural network is a relatively straightforward type of neural network that consists of an input layer, an output layer, and one or more layers of hidden neurons. In a feed-forward network, there is no feedback connection between the output and input neurons. This network can be categorized into two main types: single-layer and multi-layer networks.

- **Input node:** The input nodes in the network are responsible for transmitting input values to the next layer, known as the hidden layer. They do not perform any computation themselves but serve as a conduit for passing the input data.
- **Hidden layer:** The hidden layers play a crucial role in processing the data. They perform computations and transfer information, in the form of weights, from the input nodes to the subsequent layer, which can be another hidden layer or the output layer.
- **Output layer:** The output layer is responsible for applying the final activation function to produce the desired output format. It takes the processed information from the hidden layers and generates the network's output.

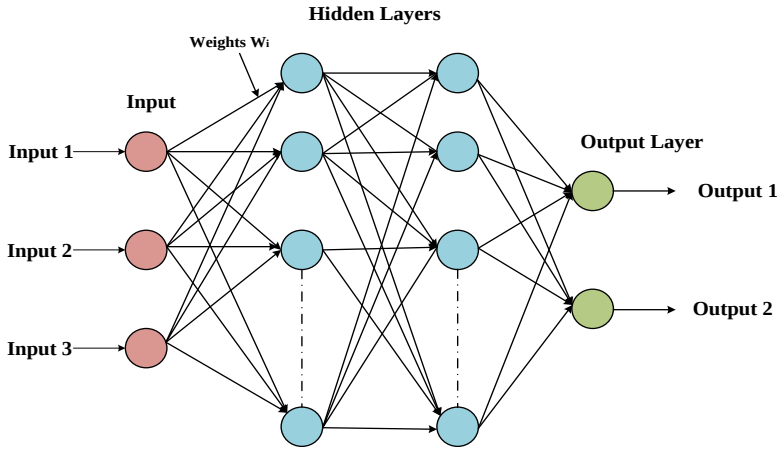

Fig. 02 Feed-forward Neural Network

MODELING OF SOLAR ARRAY

The PV (Photovoltaic) module is a technology used to convert sunlight into electricity. It serves as the fundamental unit of a solar PV system. When a PV module is exposed to solar irradiation,

it generates direct current (DC) without causing any noise or environmental impact.

Solar Cell - A solar cell is the basic building block of a solar PV system. There are various types of solar cells available, but the two main types commonly used are polycrystalline and monocrystalline cells. Solar cells are typically constructed using semiconductor materials like silicon, gallium arsenide, and cadmium telluride. They function as semiconductor diodes with a p-n junction that is exposed to sunlight. When sunlight interacts with the cell, it creates free electron and hole pairs. When the positive and negative terminals of the solar cell are connected to a DC load, current starts flowing [5].

Solar Module - A single solar cell generates a very low voltage, typically around 0.5 V. To increase the voltage and wattage output, multiple solar cells are connected together to form a solar module. By connecting solar cells in series or parallel, the voltage and power output of the module can be increased.

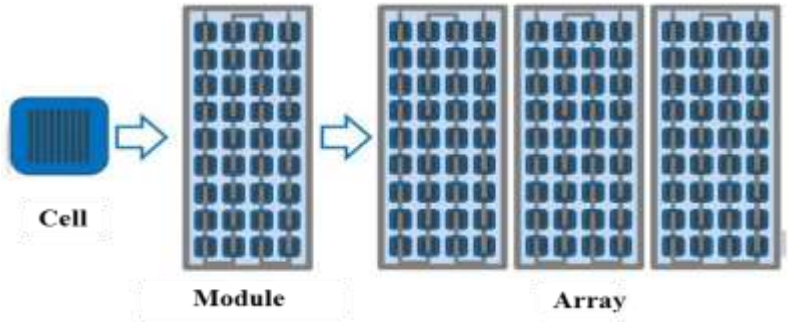

Fig. 03: PV cell, Module and PV array

Solar Array - In order to achieve the desired current and voltage levels, solar modules are connected in both series and parallel configurations. For the purpose of modeling, we have utilized the Sun Power SPR-30E-WHT-D PV array, consisting of 5 modules connected in series and 33 modules connected in parallel.

Equivalent Circuit of Solar Cell -. It consists of a light-generated current source (I_L) accompanied by a diode connected in parallel. The series resistor (R_s) represents the internal resistance of the cell, while the shunt resistance (R_sh) accounts for the leakage current [Nguyen et al., 2015].

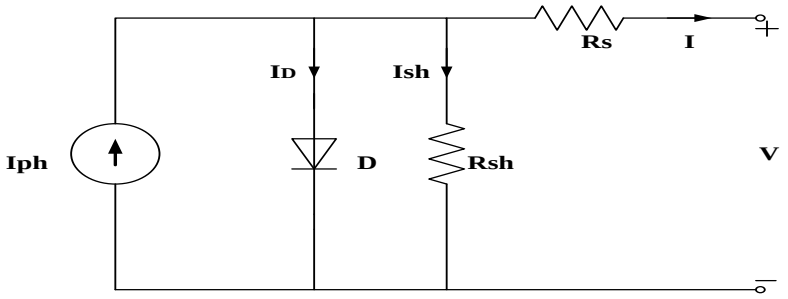

Fig. 04: Equivalent circuit diagram of solar cell

$$I(t) = I_{ph}(t) - I_D(t) - I_{sh}(t) \quad \text{....(3.1)}$$

$$I_D(t) = I_o\left(e^{\left(\frac{q(V+IR_s)}{nkT}\right)} - 1\right) \quad \text{....(3.2)}$$

$$I(t) = I_{ph} - I_o\left(e^{\left(\frac{q(V+IR_s)}{nkT}\right)} - 1\right) - \frac{V+IR_s}{R_{sh}} \quad \text{....(3.3)}$$

Where,
V: Cell output voltage,
T: Reference cell operating temperature (25 °C),
R_s: Series resistance of cell,
R_{sh}: Shunt resistance of cell,
I_{ph}: Photocurrent, function of irradiation level and junction temperature,
I_o: Reverse saturation current of the diode,
I: Cell output current,
k: Boltzmann constant (1.38 × 10-23 J/K),

q: Electron charge (1.602 × 10^-19 C),
n: Diode ideality factor.
As we discussed earlier PV cell grouped together into module and modules are grouped into series and parallel to form array which are used to generate electricity []6.

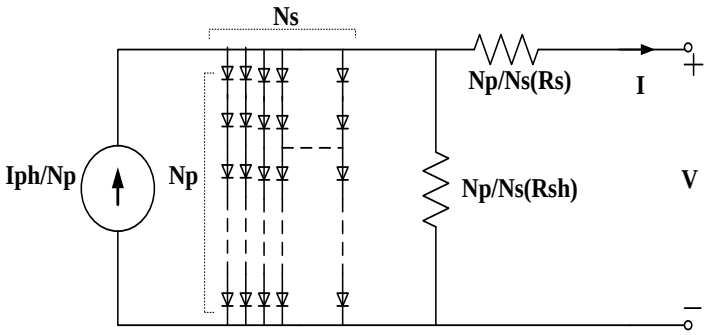

Fig. 05: Equivalent circuit of PV array

$$I(t) = N_P I_{ph} - N_P I_{ph} I_o \left(e^{\left(\frac{q(V/N_S + IR_S/N_P)}{nkT}\right)} - 1 \right) - I_{sh} \quad \text{....(3.4)}$$

$$I_{sh} = \frac{V\left(N_P/N_S\right) + IR_s}{R_{sh}} \quad \text{....(3.5)}$$

Where,
N_S : No. of cell in series,
N_P: No. of cell in parallel.

MODELING OF BOOST CONVERTER WITH MPPT CONTROLLER

In recent times, power electronics has emerged as a rapidly advancing technology. Components with higher voltage and current ratings are being developed, while losses are being reduced through the implementation of simple control circuitry [6]. Various types of converters are available, but for the purpose of this discussion, we will focus on transformerless power electronics converters, as the input in this context is in the form of DC.

The output power generated by a solar array is typically an uncontrolled low-level DC voltage. In order to minimize losses, it is necessary to step up this voltage to higher levels [7]. To achieve this, a DC-DC boost converter is employed as a front-end power electronics converter, connecting the solar array to the inverter. The boost converter plays a crucial role in enhancing the system's performance and ensuring proper coordination between the system and the utility grid. Its primary objective is to track the maximum power point of the system by regulating the system voltage, thereby optimizing power generation from the solar array.

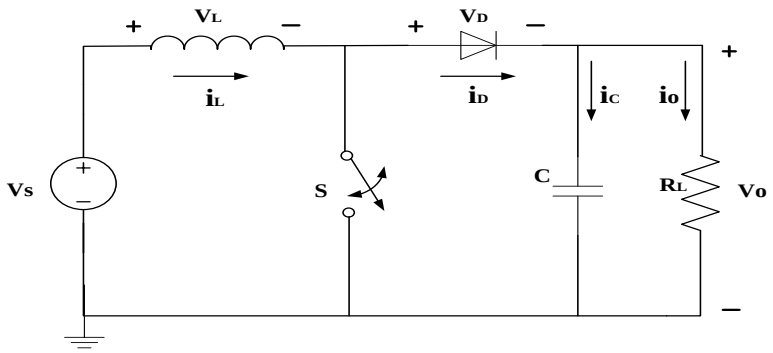

Fig. 06: Equivalent circuit of Boost Converter

It consists of an input dc voltage source, controlled switch (IGBT), diode, inductor coil, filter capacitor C. When the switch is ON, the current in the inductor increases linearly and the diode is in OFF state .When the switch is OFF the energy stored in the inductor will be released through diode to the R-load. The output voltage is

directly proportional to the duty ratio of the converter, [**Rawoof *et al*. (2015)**].

From inductor voltage balance equation:

$$V_S(DT_S) = (V_S - V_O)(1-D)T_S \quad ...(3.10)$$

$$V_O = \frac{V_S}{(1-D)} \quad ....(3.11)$$

$$\alpha = \frac{V_O}{V_S} = \frac{1}{(1-D)} \quad ....(3.12)$$

$$D = \frac{V_O - V_S}{V_O} \quad ....(3.13)$$

Where,

V_S: Input voltage,

V_O: Output voltage,

D: Duty ratio.

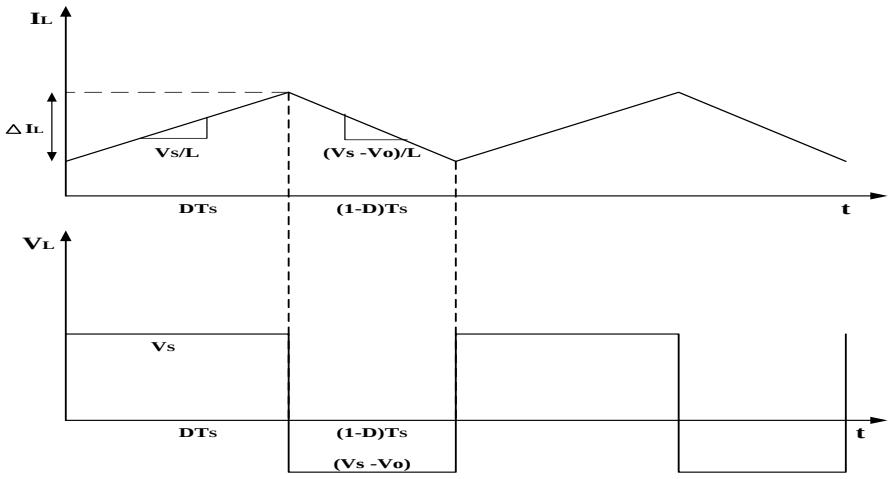

Fig. 07: Output waveforms of Boost Converter

Table 01: Parameters used in Simulation of Boost Converter

Parameter	**Value**
Inductor	$40e^{-3}$ H
Capacitor	C1 = C2 = $12000e^{-6}$ F
Input voltage	251 V
Output voltage	500 V
Input current	191 A

The V-I (Voltage-Current) characteristics of a PV (Photovoltaic) module are nonlinear, necessitating the calculation of the maximum power point to extract the maximum power under varying environmental conditions. The MPPT (Maximum Power Point Tracking) control scheme, which adjusts the duty ratio of the boost converter to control the output voltage level of the PV array. There are various techniques available to calculate the maximum power point from the output of the PV array. In this particular study, the perturb and observe (P&O) algorithm is employed for this purpose [Laamami et al., 2017].

The P&O algorithm is widely favored due to its simplicity and ease of implementation. In this method, perturbations are applied to the operating voltage of the PV array. As the P&O algorithm cannot directly compare the array terminal voltage with the actual maximum power point voltage, the change in power is considered as a result of perturbing the array terminal voltage. It is important to note that the output of this method may exhibit some oscillations, which can be mitigated by reducing the size of the perturbation [10].

The flow chart for the P&O algorithm is changes in the terminal voltage of the PV array are responsible for adjustments in the duty cycle [11]. The P&O algorithm operates periodically by increasing or decreasing the PV array voltage or current and comparing the output power P(n+1) with the previous power value P(n). If the perturbation in the terminal voltage leads to an increase in power (dp/dv=0), the perturbation is maintained in the same direction. Otherwise, it is

adjusted in the opposite direction. This cycle of perturbation is repeated until the maximum power point is reached.

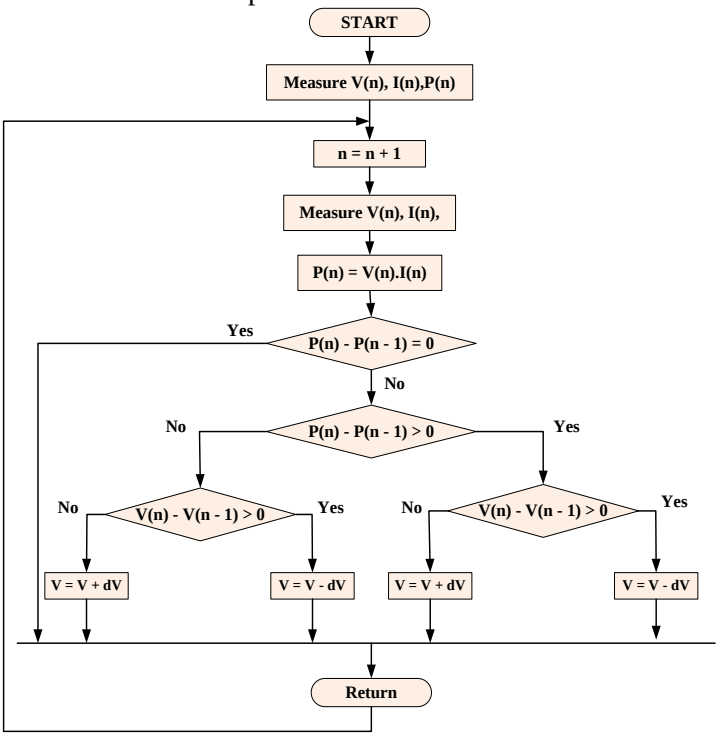

Fig. 08: Flowchart of MPPT algorithm

MODELING OF INVERTER

The PV array is connected to the utility grid, which maintains a voltage of 25 kV through a three-phase, 12-pulse converter. An inverter is employed to convert the DC voltage from the PV array into AC voltage. The inverter must supply a voltage higher than that of the utility grid to ensure power flow in the direction of the grid. Synchronization is of great importance for PV inverters. PWM (Pulse Width Modulation) approaches are utilized to control the switching of the semiconductor switches. There are various techniques available to control the voltage and current of the inverter, with the PI (Proportional-Integral) controller being the most commonly used controller [11].

To connect the power plant to the grid, the output voltage of the inverter must have the same frequency as the utility grid. This is achieved through the use of a current controller with a Phase-Locked Loop (PLL). Figure 3.7 depicts an inverter with a current control controller for grid synchronization. This synchronization is accomplished by transforming the three-phase voltage and current into a rotating reference frame (dq0) using Park's transformation. The transformed quantities are then converted back into three-phase reference quantities. Park's transformation is employed to convert the ABC components into three constant DC quantities, namely the direct, quadrature, and zero components. These constant DC quantities can be easily regulated using a PI controller. The ABC to dq0 transformation is carried out using the equation described below.

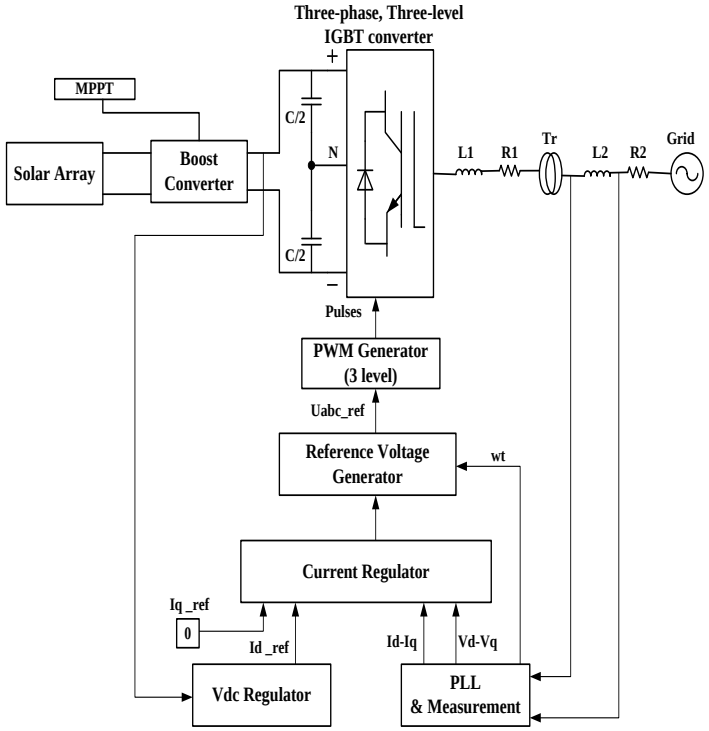

Fig. 09: Grid Synchronization of three-phase inverter

$$\begin{bmatrix} U_d \\ U_q \\ U_0 \end{bmatrix} = \frac{2}{3}\begin{bmatrix} \cos wt & \cos(wt - {}^{2\pi}/_{3}) & \cos(wt - {}^{2\pi}/_{3}) \\ -\sin wt & -\sin(wt - {}^{2\pi}/_{3}) & -\sin(wt - {}^{2\pi}/_{3}) \\ \frac{1}{2} & \frac{1}{2} & \frac{1}{2} \end{bmatrix}\begin{bmatrix} U_a \\ U_b \\ U_c \end{bmatrix} \quad \text{....(3.14)}$$

Grid voltage and current are uncontrolled quantities, most feasible approach of controlling the operation is by *Iq* and *Id* control. Figure shows controller used for voltage and current of inverter.

$$e_d = I_{d\_ref} - I_d \quad \text{....(3.14)}$$

Similarly the output of another controller is

$$e_q = I_{q\_ref} - I_q \quad \text{....(3.15)}$$

Both error signal e_d and e_q are processed by PI regulator. Constant of PI regulator are chosen such as

$$K_p = {}^{L}/_{\tau_i} \quad \text{....(3.16)}$$

$$K_i = {}^{R}/_{\tau_i} \quad \text{....(3.17)}$$

Here, L and R represent the inductance and capacitance of distribution system. τ_i is time constant of current control loop. PLL is a feedback system with PI regulator used to track phase angle of utility grid

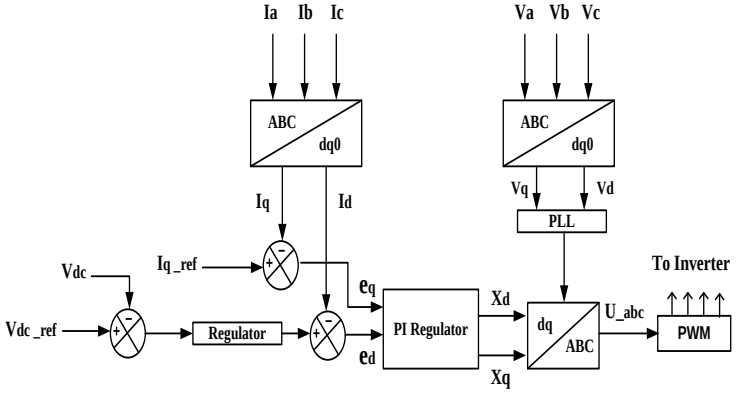

Fig. 10: Current Controller of Inverter with PLL

Sinusoidal pulse width modulation:
The inverter plays a crucial role in converting a constant DC input voltage into a controlled AC output voltage by controlling the switching of semiconductor switches. To achieve this control, the sinusoidal pulse width modulation technique (SPWM) is employed to manipulate the gate circuitry of the inverter. The SPWM technique utilizes constant amplitude pulses, and the width of these pulses can be adjusted to control the output voltage and minimize lower-order harmonics.

SPWM is widely used in industrial converters due to its effectiveness. In the general principle of SPWM, an isosceles triangular carrier wave with a carrier frequency (fc) is compared with the fundamental frequency (fm) of a sinusoidal modulating wave [12]. The SPWM modulating signals are generated by converting the dq components into abc components and comparing the carrier frequency (fc) with the grid angular frequency (ω). This process allows for precise control of the inverter's output voltage and facilitates synchronization with the grid.

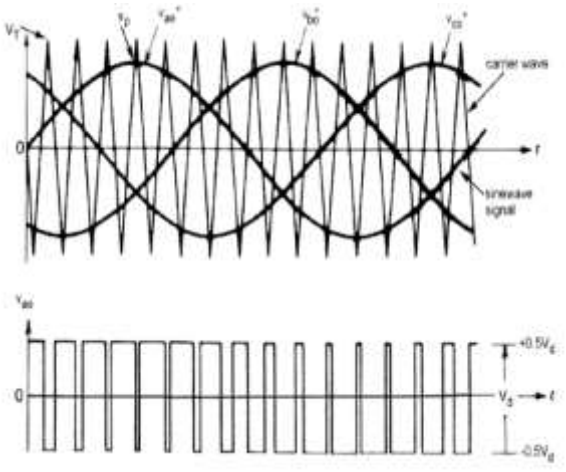

Fig. 11: Principle of SPWM

The working of Sinusoidal Pulse Width Modulation (SPWM) can be described based on the following points:

- The frequency of the triangular wave used in SPWM corresponds to the frequency of the Pulse Width Modulation (PWM) signal.
- The fundamental frequency of the system is controlled by the frequency of the controlled voltage.
- The amplitude of the output voltage is determined by the peak value of the control voltage.
- The modulating index of the inverter is defined as the ratio between the peak magnitude of the modulating waveform and the carrier wave.

MATLAB/SIMULINK MODEL OF GRID CONNECTED SOLAR PV SYSTEM
A 50-kW photovoltaic (PV) array is connected to a 25-kV utility grid through a DC-DC boost converter and a Voltage Source Inverter (VSI). The Maximum Power Point Tracking (MPPT) algorithm is implemented using the Perturb and Observe method in the boost converter to extract maximum power from the PV array [13]. For grid synchronization, a current controller with a Phase Lock Loop (PLL) is utilized in the inverter.

The Simulink model of the 50-kW grid-connected solar PV system, includes the following components:

1. PV array: The system employs SunPower SPR-305E-WHT-D modules with a total capacity of 50 kW. The PV array block takes two inputs: irradiance in W/m² and temperature in degrees Celsius.
2. Boost Converter: This component increases the output voltage of the PV array from 251 V to 500 V. The duty ratio of the boost converter is automatically adjusted by the MPPT controller to maximize power extraction from the PV array [13].
3. Voltage Source Inverter: The inverter converts the 500 V DC output voltage of the boost converter into a balanced +/-250 V AC output with a unity power factor. The current controller, in conjunction with the PLL, ensures synchronization with the utility grid.
4. 10-kVAR Capacitor Bank: This capacitor bank is employed to mitigate the harmonics generated by the inverter.
5. 100-kVA 250V/25kV Three-Phase Coupling Transformer: This transformer is utilized to connect the solar system to the utility grid.
6. Utility Grid: The utility grid is a 25-kV distribution feeder that is equivalent to a 120-kV transmission system.

These components work together to enable the grid-connected operation of the 50-kW solar PV system while ensuring synchronization with the utility grid and maximizing power extraction from the PV array.

Table 02: Parameter used in Simulation PV module named Sun Power SPR-305E-WHT-D.

Parameter	**Values used for Simulation**
Maximum Power (Pm)	305.226 W
Short-circuit current (**Isc**)	5.96 A
Open-circuit voltage (**Voc**)	64.2 V
Voltage at maximum power point (**Vmp)**	54.7 V
Current at Maximum power point (**Imp)**	5.58 A
Temperature coefficient of Isc (**Ki**)	-0.27269 $\%/^{\circ}C$
Temperature coefficient of Voc (**Kv**)	0.061745 $\%/^{\circ}C$
N_S	33
N_P	5

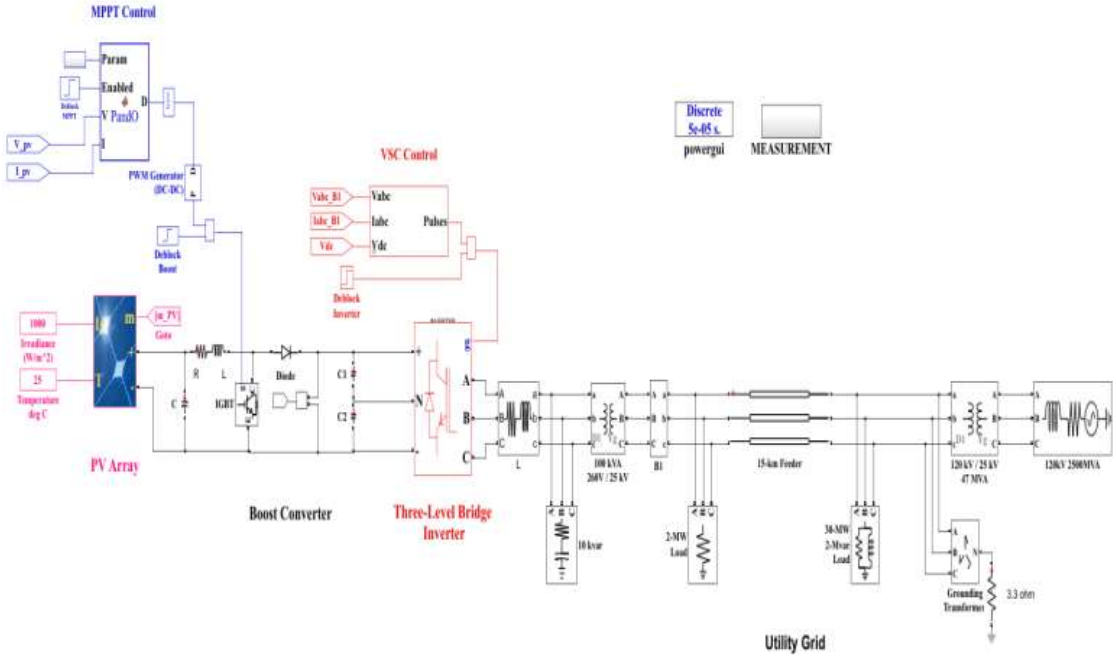

Fig. 12: Simulink Model of 50-kW Grid-connected Solar PV System (detailed model)

Simulation of neural fitting tool

For this project, we utilized the nfstart tool in MATLAB, which consists of four main tools:

1. Fitting app (nftool): This tool is employed for creating a neural network that maps numeric input data to numeric output data.
2. Pattern recognition app (nprtool): This tool is utilized for training a neural network that can classify input data into specific output categories.
3. Clustering app (nctool): This tool is employed for grouping data based on their similarity using a neural network approach.
4. Time series app (ntstool): This tool is specifically designed for nonlinear filtering and prediction of future values in time series data. It utilizes past values of the time series to predict future values.

In our project, we focused on fault detection using neural networks. Electrical faults can result in changes in voltage, current, and impedance within the power system. For training the neural network, we selected voltage data from all three phases of the transmission line [14]. We collected a total of 28,003 fault samples for training purposes. Table 3 displays a sample of the input database used in the neural fitting tool, which consists of voltage values ( ) of the transmission line as input and two output values: 1 for a healthy condition and 2 for a faulty condition.

Table 03: Input training dataset for fault detection of transmission line

Voltage V_A	**Voltage V_B**	**Voltage V_C**	**Output**
-99.5254	-199.15	298.6759	1
-94.9897	-202.74	297.7301	1
-90.4251	-206.286	296.7116	1
-85.8345	-209.783	295.6177	1

-81.2165	-213.23	294.4465	1
-76.5694	-216.631	293.2009	1
-71.8975	-219.99	291.8872	1
-67.2099	-223.297	290.5065	1
-62.514	-226.54	289.054	1
-57.8113	-229.715	287.5262	1
-53.1002	-232.826	285.9265	1
-48.3801	-235.882	284.2622	1
-43.6535	-238.884	282.5372	1
-38.9224	-241.826	280.748	1
-34.1866	-244.7	278.8869	1
-29.4454	-247.505	276.9509	1
-29.5119	-247.39	276.9022	2
-23.1888	-234.096	257.2849	2
-15.8941	-207.79	223.6836	2
-10.8866	-198.767	209.6536	2
-9.16513	-220.655	229.8201	2
-7.10428	-243.121	250.2257	2
-1.88558	-237.805	239.6902	2
4.381137	-220.347	215.9659	2
8.532672	-220.233	211.7	2
10.74136	-239.264	228.5222	2
13.99571	-251.162	237.1664	2
19.34467	-243.885	224.5405	2
24.83121	-233.304	208.473	2
28.52933	-238.201	209.6718	2
31.36154	-252.397	221.0356	2
35.30328	-257.798	222.495	2
-303.92	140.3493	163.5705	1
-303.653	136.0963	167.5568	1
-303.313	131.8078	171.5054	1
-302.903	127.4869	175.4159	1
-302.423	123.1323	179.2912	1
-301.869	118.7484	183.1201	1
-301.237	114.3346	186.9026	1

The input data set used in this project is divided into three separate parts:

1. Training set: This portion of the data is used to train the neural network by adjusting the weights and biases. During the training process, the network's error is minimized. In our case, we allocated 70% of the input data (19,603 samples) for training.

2. Validation set: This set of data is used to assess the performance of the neural network on patterns that were not included in the training phase. It helps in tuning the hyperparameters of the system. We allocated 15% of the input data (4,200 samples) for validation.

3. Testing set: This set of data is used to evaluate the overall performance of the neural network after training and validation. It provides a final check on the network's performance. We allocated 15% of the input data (4,200 samples) for testing.

For simulation purposes, we utilized a two-layer feed-forward neural network.. The activation functions used in the network are described by Equation (3.32) for the linear activation function and Equation (3.33) for the sigmoid activation function.

$$F(x) = x \quad \text{....(3.32)}$$

$$F(x) = \frac{1}{1 + e^{-x}} \quad \text{....(3.33)}$$

$$E = \frac{1}{2}\sum k\ (e_k)^2 = \frac{1}{2}\|e\|^2 \quad \text{....(3.34)}$$

where, e_k is error in k^{th} pattern, e is a vector with element e_k. If the difference between previous weight vector and next weight vector is very small, the error can be expanded by Taylor series.

$$(j+1) = e(j) + \frac{\partial e_k}{\partial w_i}[w(j+1) - w(j)]\, e \quad \text{....(3.35)}$$

As a outcome, error function can be expressed as

$$E = \frac{1}{2}\ \|e(j) + \partial e_k/\partial w_i\ [w(j+1) - w(j)]\|^2 \quad \text{....(3.36)}$$

minimization of the error function with respect to new weight vector, gives

$$w(j+1) = w(j) - (Z^T Z)^{-1} Z^T e(j) \quad \text{....(3.37)}$$

Where $(Z)k_i = \partial e_k/\partial w_i$

since, Hessian for some of square error function is

$$(H)_{ij} = \frac{\partial^2 E}{\partial w_i \partial w_j} = \sum\{\left(\frac{\partial e_k}{\partial w_i}\right)\left(\frac{\partial e_k}{\partial w_i}\right) + e_k \partial^2 e_k/\ \partial w_i \partial w_j\} \quad \text{....(3.38)}$$

by neglecting second term, Hessian can be written as

$$H = Z^T Z \quad \text{....(3.39)}$$

Hessian matrix is easy to compute because it is based on the first order derivative, it can be easily accommodate by back propagation. Hessian weight updating formula can be applied as iteratively to reduce error function, this may result in large step size, which would invalidated liner approximation.

In Levenberg-Marquart back propagation algorithm, error function is minimized, while the step size is kept small in order to ensure the validity of liner approximation. The modified error function is given by Equation (3.40).

$$E = \frac{1}{2}\|e(j) + \partial e_k/\partial w_i\ [w(j+1) - w(j)]\|^2 + \gamma\|\ [w(j+1) - w(j)]\|^2 \quad \text{....(3.40)}$$

where, γ is step size governing parameter. Minimizing the modified error with respect to $w(j+1)$ gives

$$w(j+1) = w(j) - (Z^T Z + \gamma I\ )^{-1} Z^T\ e(j) \quad \text{....(3.41)}$$

It is specially designed for curve fitting problems where training stopped automatically when generalization stops improving. Figure shows training results of neural network.

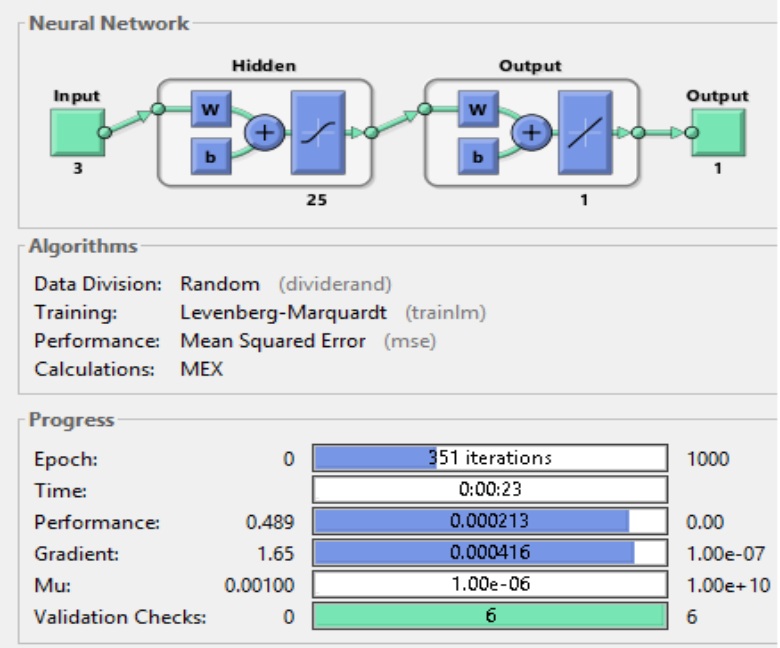

Fig. 13: Results of training of neural network

If network is not successfully train, we can retrain the network with same input and output parameters. Second approach, we can increase no. of hidden neurons which gives more flexibility in optimization of neural network

MATLAB/SIMULINK MODEL OF 50-kW SOLAR PV SYATEM WITH FRT

This study focuses on a 50-kW solar array that is connected to a 25-kV grid using a boost converter with MPPT controller. Additionally, a voltage source inverter (VSI) with a current control loop is implemented to ensure effective synchronization of the inverter voltage and frequency with the grid. A coupling transformer is used to connect the system to the load and utility grid. Furthermore, a DSTATCOM consisting of a six-pulse converter is connected to a 25-kV line to enable fault ride-through capability. The main objective is to analyze the impact of faults on the system with and without the DSTATCOM.

To assess the performance of the system with the implemented control scheme, simulations were conducted using MATLAB R2017a software. This section presents the comprehensive simulation model of the grid-connected solar system with a neural network for fault detection and the DSTATCOM for fault ride-through capability.

The Simulink model of the grid-connected solar system incorporating the neural network for fault detection and the DSTATCOM for fault ride-through. The simulation results are analyzed to evaluate the system's performance [14].

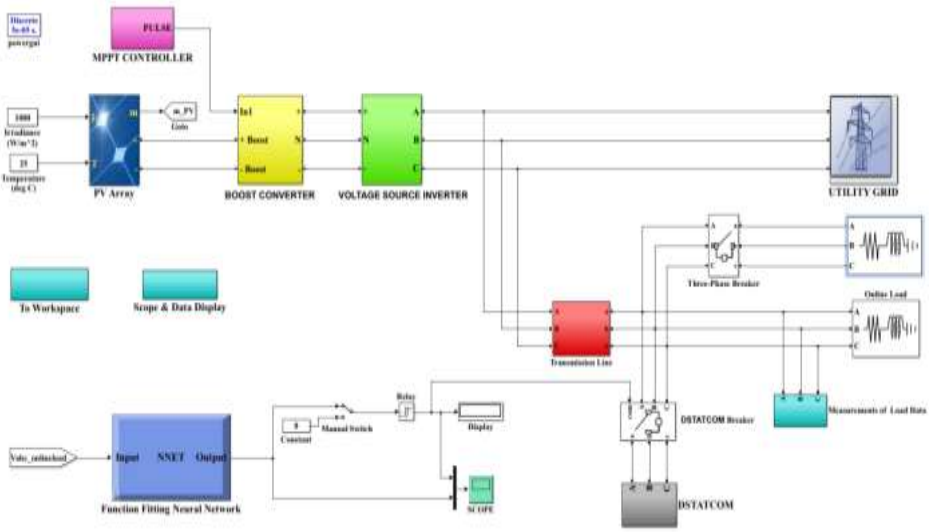

Fig. 14: Simulink Model of 50 kW Grid-connected Solar PV System with Neural Network Tool and DSTATCOM

OUTPUT WAVEFORMS OF GRID CONNECTED SOLAR PV SYSTEM

MATLAB/Simulink Results of PV Array

Here the Simulation is carried out under Standard Test Conditions (STC) with module temperature of 298 K (25 ºC) and irradiance of 1000 W/m2.

The behavior of PV array, as temperature increases the output voltage of PV array decreases and current generated by PV array increases with increase of irradiation falling on PV array.

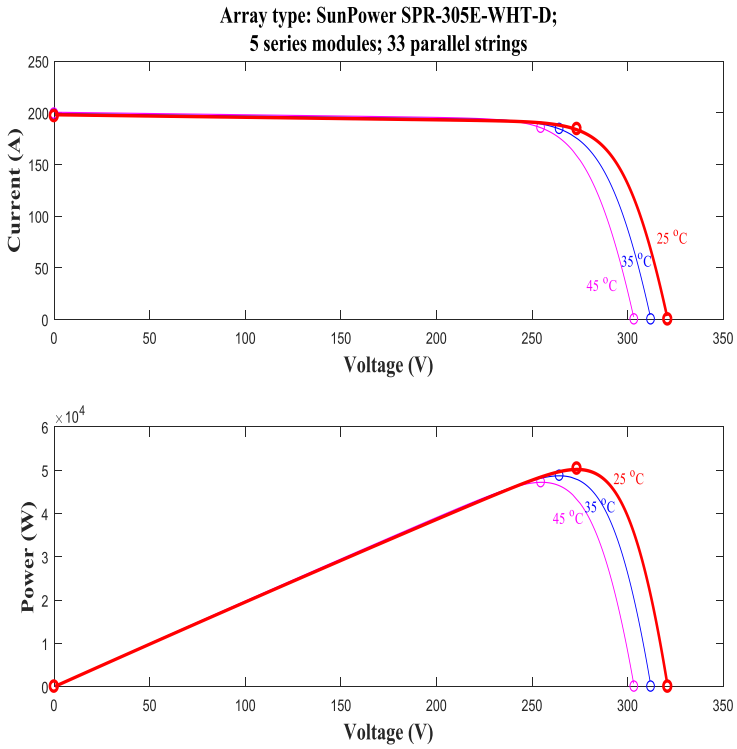

Fig. 15: I-V and P-V Characteristics of PV Array at constant Irradiance (1000 W/m^2) and Variable Temperature

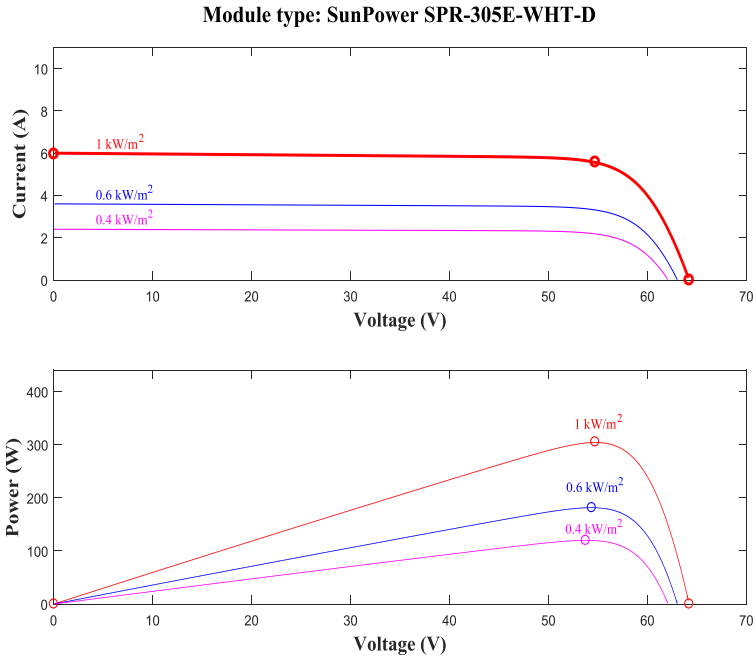

Fig. 15: I-V and P-V Characteristics of PV Array at Constant Temperature (25 ºC) and Variable Irradiance

Here the Simulation results of PV array are presented and voltage of PV array which are respectively 191 A and 251 V.

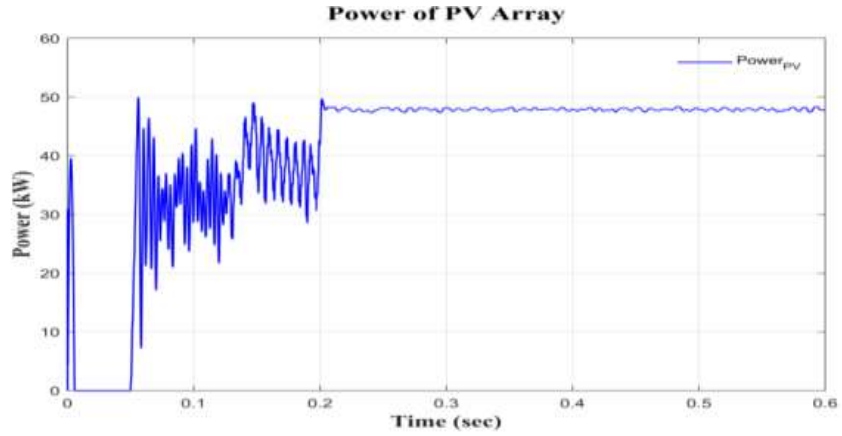

Fig. 16: Output Power waveform of PV array

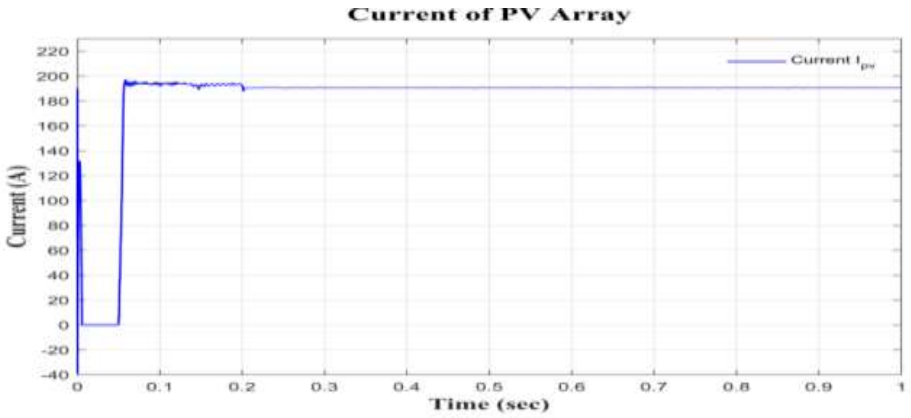

Fig. 17: Output Current Waveform of PV array

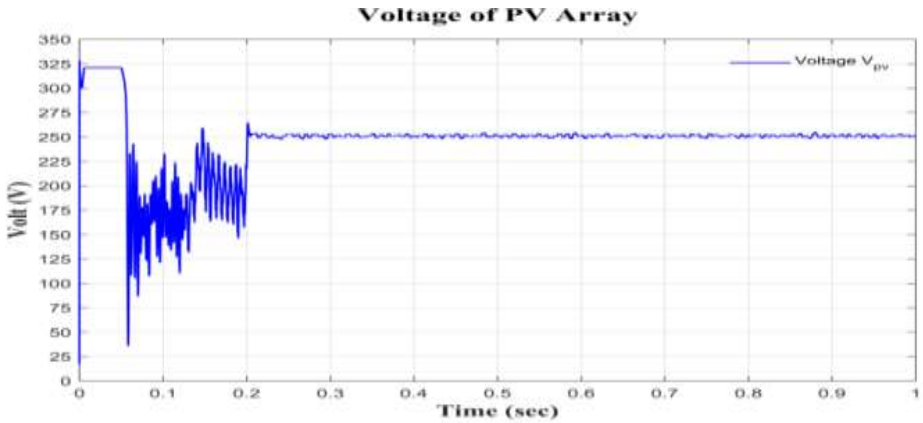

Fig. 18: Output Voltage Waveform of PV array

MATLAB/Simulink results of Boost Converter and MPPT Controller

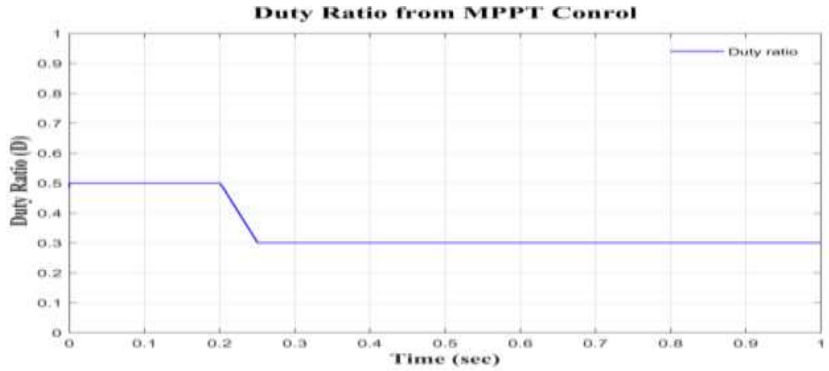

Fig. 19: Duty Ratio Generated by Maximum Power Point Tracking Algorithm

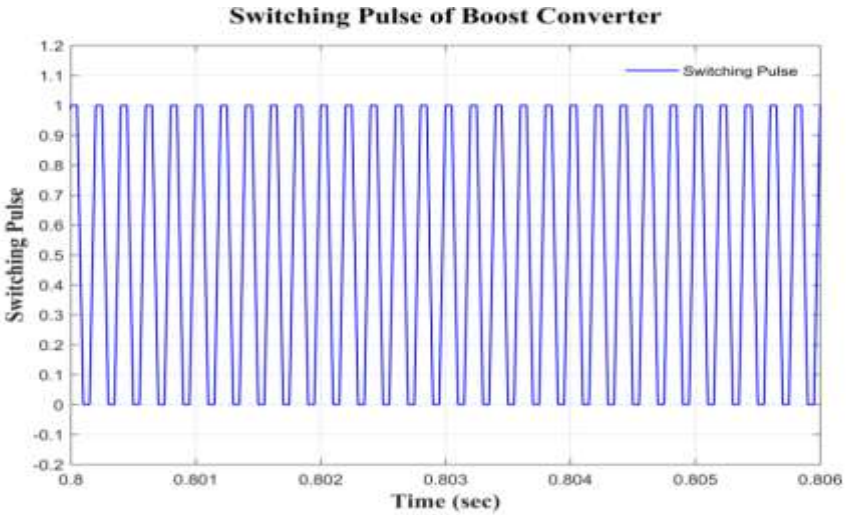

Fig. 20: Switching Pulses for IGBT of Boost Converter

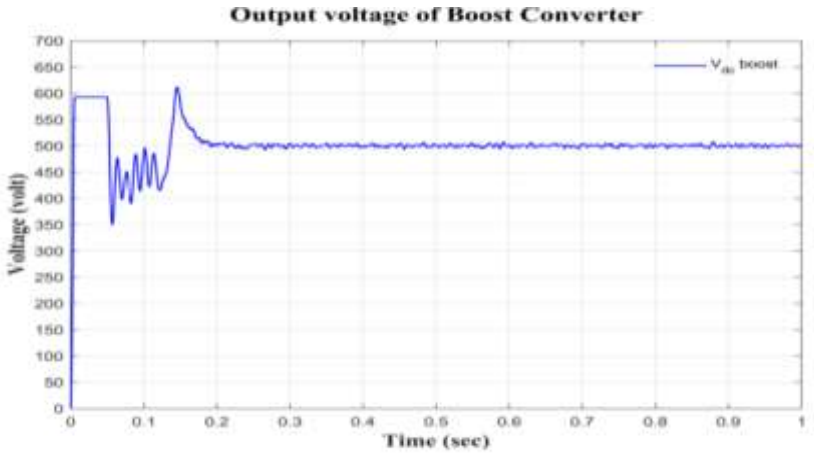

Fig. 21: Output voltage waveform of Boost Converter

In Figures above shows respectively input and output of boost converter. Output voltage of PV array is 251V which is step up by the boost converter to 500V.

MATLAB/Simulink results of Voltage Source Inverter

Simulation results of three-level power inverter are shown. Figure 4.10 shows the modulation index of inverter vary between 0.8 to 0.9.

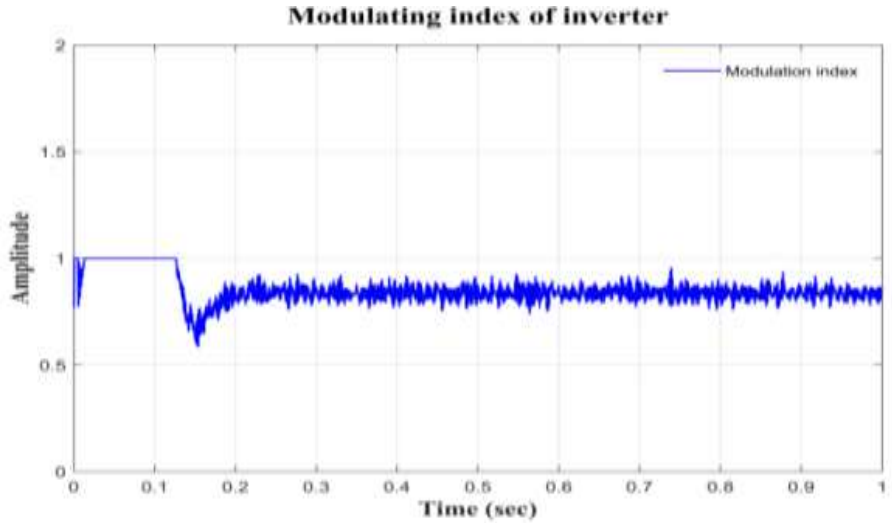

Fig. 22: Modulating Index of Voltage source inverter

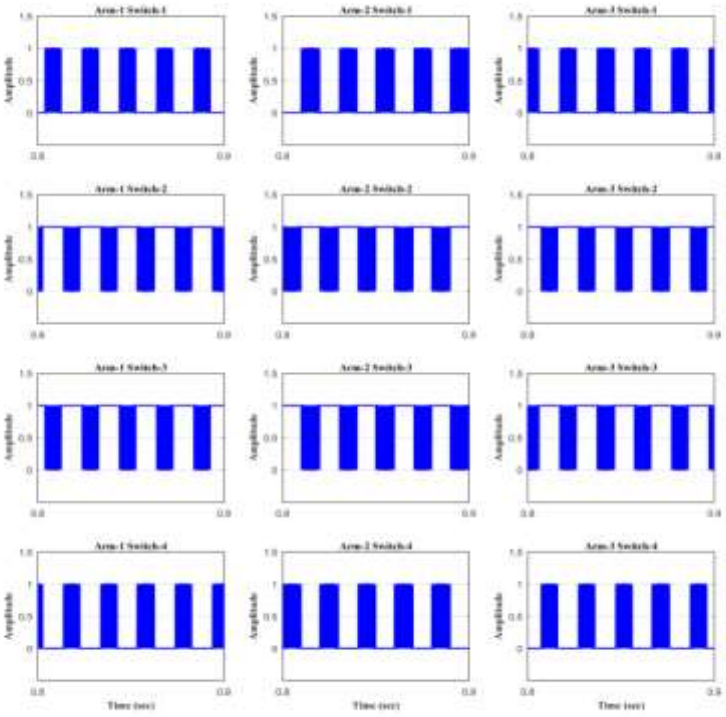

Fig. 23: Switching Pulses of Three Level Bridge Inverter

The combined switching pulses of each IGBT of the three level bridge inverter, each arm consist of four switches.

The output voltage and current waveforms of the inverter are presented in this section, specifically the line-to-line voltage, a zoomed-in view of the line-to-line voltage, and the three-phase output voltage. It can be observed that the line-to-line voltage is approximately 500 V and exhibits a stepped waveform instead of a purely sinusoidal shape [15]. Furthermore, the three-phase output current waveform of the inverter, revealing the presence of harmonics in the waveform due to total harmonic distortion.

SUMMERY AND CONCLUSION

In this study, a fault detection and fault ride-through technique for a grid-connected solar PV system was developed using MATLAB/Simulink R2017a. The system consists of a 50-kW PV array, boost converter, voltage source inverter, and utility grid. A controlling circuit was implemented to regulate the operation of the DSTATCOM under different system conditions. An online fault detection technique utilizing artificial neural network was developed using the neural fitting tool in MATLAB/Simulink [15].

The performance of the system was evaluated under various load conditions, and the following conclusions were drawn:

1. A 50-kW grid-connected solar PV system was successfully implemented in MATLAB/Simulink.
2. An online fault detection technique using neural fitting tool was developed and integrated into the simulation environment.
3. Simulations were conducted for three-phase faults, and the DSTATCOM was utilized to improve the fault ride-through (FRT) capability of the solar system. The results indicated that during a fault, the system voltage decreased below its nominal value. However, when a voltage swell occurred, the DSTATCOM automatically connected to the grid and provided reactive power compensation, leading to the restoration of the voltage to its nominal value.
4. The system was tested under various load conditions, including full load, half load, and no load. In the absence of DSTATCOM for fault ride-through, the line-to-line voltage deviated from its nominal value. However, when the DSTATCOM was connected to the grid, the line voltage returned to its nominal value.
5. A three-level, 12-pulse voltage source inverter was employed, along with a grid synchronization controller based on the phase-locked loop (PLL) technique and a current controller.

Overall, the developed system and control scheme demonstrated promising performance in fault

detection and fault ride-through for grid-connected solar PV systems.

FUTURE SCOPE

Based on the literature reviewed and the scope of the paper, there are several areas that can be explored and implemented in the existing model:

1. Enhancement of DSTATCOM Efficiency: The efficiency of the DSTATCOM can be improved by designing the Voltage Source Converter (VSC) with a higher number of output levels. This can lead to improved performance and better voltage regulation during fault conditions.

2. Utilization of Solar Inverter for Reactive Power Supply: The solar inverter can be utilized not only for converting DC to AC power but also for supplying reactive power to the grid. By implementing suitable control strategies, the solar inverter can contribute to the power factor correction and reactive power compensation in the grid-connected system.

3. Application of Artificial Intelligence Techniques for Fault Detection and Circuit Reconfiguration: Different artificial intelligence-based techniques, such as fuzzy logic and neuro-fuzzy systems, can be employed to identify the type of fault and reconfigure the circuit more efficiently and quickly. These techniques can enhance the fault detection accuracy and enable faster response and improved system reliability.

REFERENCES

1. Arani, M.S. and Heiazi, M.A. 2016. The comprehensive study of electrical fault in PV arrays. *Journal of Electrical and Computer Engineering* : pp. 1-10.
2. Arya, J. and Saini, L.M. 2014. Single stage single phase solar inverter with improved fault ride through capability. *IEEE 6th India International Conference on Power Electronics (IICPE)* held during December 8-10, 2014, pp. 1-5.
3. Azevedo, G.M.S., Vazquez, G., Luna, A., Aguilar, D. and Rolan, A. 2009. Photovoltaic inverter with fault ride through capability. *IEEE International Symposium on Industrial Electronics* held during July 5-8, 2009, pp. 549-553.
4. Badi, L.W.A., Zakaria, Z., Nordin, A.H.M. and Mustapa, R.F. 2014. Fault analysis in grid connected PV system. *IEEE International Conference Power and Energy (PE Con)* held during December 1-3, 2014, pp. 360-365.
5. Banu, I.V. and Istrate, M. 2014. Study on three phase photovoltaic system under grid faults. *IEEE International Conference and Exposition on Electrical and Power Engineering* held during October 16-18, 2014, pp.1132-1137.
6. Benz, C.H., Franke W.T. and Funchs, F.W. 2010. Low voltage ride through capability of a 5-KW grid-tied solar inverter. *Proceedings of 14th International Power Electronics and Motion Control Conference EPE-PEMC* held during September 6-8, 2010, pp. T12-13 - T12-20.
7. Bhat, S. and Ballal, R. 2017. MATLAB/Simulink based design and development of 5KW solar PV-grid connected power system; trends and challenges. *International Conference on Circuit, Power and Computing Technologies (ICCPCT)* held during April 20-21, 2017, pp. 1-7.
8. Chhikara, R., Dua, D. and Mehta, N. 2015. Review paper on the grid connected PV system and related problems. *International Journal of Engineering Science and Research Technology* **4** : 516-522.
9. Choudhury , S.R., Gupta, A. and Anand, S. 2016. Simulation of low voltage ride through scheme for inverter connected to distribution system with high R/X ratio. *IEEE 10th International Conference on Compatibility, Power electronics and Power engineering (CPE POWER ENG)* held during June 29-July 1, 2016, pp. 202-207.
10. Chunlai, L. and Xianshung, Z. 2016. A survey of online fault diagnosis for PV module Based on BP neural network. *2016 International Conference on Smart city and System Engineering(ICSCSE)* held during November 25-26, 2016, pp. 483-486.
11. Dhimish, M., Holmes, V., Mehrdadi, B. and Dales, M. 2017. Simultaneous fault detection algorithm for grid connected photovoltaic plants. *IEEE Transaction on IET Renewable Power Generation* **11** : 1565-1575.
12. Eberlin, M., Seidle, C. and Reichert, S. 2014. Innovative state - space controller for an optimized low voltage - ride - through behaviour. *16th European Conference on Power Electronics and Application* held during August 26-28, 2014, pp. 1-8.
13. Fujii, K., Kanao, N., Yamada, T., and Okuma, Y. 2011. Fault ride through capability for solar inverter. *Proceedings of the14th European conference on Power Electronics and Application* held during August 30-September 1, 2011, pp. 1-9.

14. Garoudja, E., Kara, K., Chouder, A., Silvestre, S. and Kinchou, S. 2016. Efficient fault diagnosis procedure for photovoltaic system. *8th International Conference on Modelling, Identification and Control* : pp. 851-856.
15. Hota, P.K., Panda, B. and Panda B. 2016. Fault analysis of grid connected photovoltaic system. *American Journal of Electrical Power and Energy System* **5** : 35-44.